Link to publication

University of Bath

Ionospheric data assimilation and forecasting during storms

Alex T. Chartier[1], Tomoko Matsuo[2], Jeffrey L. Anderson[3], Nancy Collins[3], Timothy J. Hoar[3], Gang Lu[4], Cathryn N. Mitchell[5], Anthea J. Coster[6], Larry J. Paxton[1], and Gary S. Bust[1]

[1]Johns Hopkins University Applied Physics Laboratory, Laurel, Maryland, USA, [2]Cooperative Institute for Research in Environmental Sciences, University of Colorado Boulder, Boulder, Colorado, USA, [3]Institute for Mathematics Applied to Geosciences, National Center for Atmospheric Research, Boulder, Colorado, USA, [4]High Altitude Observatory, National Center for Atmospheric Research, Boulder, Colorado, USA, [5]Dept. Electrical Engineering, University of Bath, Bath, UK, [6]MIT Haystack Observatory, Westford, Massachusetts, USA

Abstract Ionospheric storms can have important effects on radio communications and navigation systems. Storm time ionospheric predictions have the potential to form part of effective mitigation strategies to these problems. Ionospheric storms are caused by strong forcing from the solar wind. Electron density enhancements are driven by penetration electric fields, as well as by thermosphere-ionosphere behavior including Traveling Atmospheric Disturbances and Traveling Ionospheric Disturbances and changes to the neutral composition. This study assesses the effect on 1 h predictions of specifying initial ionospheric and thermospheric conditions using total electron content (TEC) observations under a fixed set of solar and high-latitude drivers. Prediction performance is assessed against TEC observations, incoherent scatter radar, and in situ electron density observations. Corotated TEC data provide a benchmark of forecast accuracy. The primary case study is the storm of 10 September 2005, while the anomalous storm of 21 January 2005 provides a secondary comparison. The study uses an ensemble Kalman filter constructed with the Data Assimilation Research Testbed and the Thermosphere Ionosphere Electrodynamics General Circulation Model. Maps of preprocessed, verticalized GPS TEC are assimilated, while high-latitude specifications from the Assimilative Mapping of Ionospheric Electrodynamics and solar flux observations from the Solar Extreme Ultraviolet Experiment are used to drive the model. The filter adjusts ionospheric and thermospheric parameters, making use of time-evolving covariance estimates. The approach is effective in correcting model biases but does not capture all the behavior of the storms. In particular, a ridge-like enhancement over the continental USA is not predicted, indicating the importance of predicting storm time electric field behavior to the problem of ionospheric forecasting.

1. Introduction

Ionospheric forecasting is challenging because the variability of the geophysical system is largely dependent on influences from the thermosphere (itself forced by the lower atmosphere), the magnetosphere, and EUV sunlight. These drivers of ionospheric behavior are especially difficult to predict during storms, so we cannot rely on having accurate knowledge of them in advance. Empirical ionospheric forecasts have been published by *Tulunay et al.* [2006], *Habarulema et al.* [2011], *Jakowski et al.* [2011], and others. Utah State University's Global Assimilation of Ionospheric Measurements (GAIM) has an ionospheric forecasting capability that uses a global, physics-based ionospheric model with specified thermospheric parameters [*McNamara et al.*, 2007], the results of which are available through NASA's Community Coordinated Modeling Center. *Cander* [2015] shows that neural networks can predict quiet time ionospheric behavior accurately at ionosonde stations, but that they falter somewhat during extreme solar events. This study presents storm time ionospheric predictions from a global, physics-based, coupled thermosphere-ionosphere ensemble data assimilation scheme that ingests TEC observations, adjusts thermospheric and ionospheric parameters, and facilitates forecasting of TEC. Comparisons are performed in the continental USA, where many observations are available and the model and observations are likely to be more reliable.

1.1. Ionospheric Storms

Buonsanto [1999] provides a comprehensive review of ionospheric storms. The ionospheric electron density is a function of solar flux, neutral composition, and dynamical effects due to neutral winds and electric fields. During geomagnetic storms, intense electric fields are mapped from the magnetosphere along geomagnetic field lines

to the high-latitude ionosphere. These electric fields cause rapid convection at high latitudes and sometimes penetrate to low latitudes. The high-latitude plasma convection drives neutral winds and heating through ion-neutral collisions. Both positive and negative effects can be seen in the ionospheric electron density at midlatitudes during storms. In the main phase of storms, increased electron densities are caused primarily by equatorward neutral winds blowing plasma upward along geomagnetic field lines, where recombination is slower. In the recovery phase, decreased electron densities are caused by atomic oxygen depletions and molecular nitrogen enhancements that result in reduced production rates. The recent work of *Borries et al.* [2015] quantifies the storm time TEC response to interplanetary magnetic field (IMF), season, and local time and highlights the important role of winds and composition in translating these drivers into TEC variations.

1.2. Forecasting

Data assimilation techniques combine model forecasts with observations to improve the estimate of the state of a geophysical system. In meteorology, the fundamental limitation to forecast accuracy is related to the sensitivity of model dynamics to initial conditions, so it is possible to produce good forecasts by combining an accurate specification of the initial state of the dynamical system with a sophisticated numerical model [*Kalnay*, 2003]. The ionosphere is not self-contained to the degree that the lower atmosphere is, so the effect of ionospheric data assimilation on forecast accuracy is often inherently limited by the variability of external drivers. As *Chartier et al.* [2013] indicated in a simulation study, knowledge of the initial ionospheric state can only improve storm time forecasts for periods of a few hours in situations where the solar, magnetospheric and thermospheric drivers are not known accurately. However, the ionospheric electron density is comparatively easier to observe than these drivers thanks to advances in remote sensing techniques. If it is possible to infer knowledge of thermospheric, magnetospheric, and solar behavior from ionospheric observations, then that is likely to substantially improve forecast accuracy using ionospheric data assimilation. Several authors [e.g., *Pi et al.*, 2003; *Codrescu et al.*, 2004; *Matsuo et al.*, 2013] have explored the possibility of forcing parameter estimation from ionospheric observations. In this study, we estimate several thermospheric and ionospheric parameters from ionospheric observations.

1.3. Thermospheric and Ionospheric Models

Given that the state of the ionosphere is largely determined by external influences, especially during storms, accurate knowledge of the temporal evolution of those external influences from the magnetosphere and Sun is essential to producing good ionospheric forecasts. Ideally, the entire geophysical system, from the Earth to the Sun, would be represented in a single coupled model, but technical and computational limitations mean that this is not currently feasible. Instead, it is necessary to draw boundaries around the areas that exhibit strong mutual coupling. From a modeling perspective, the most common approach has been to couple the thermosphere with the ionosphere [*Roble et al.*, 1988; *Fuller-Rowell et al.*, 1996; *Ridley et al.*, 2006], although there have been more recent developments in whole atmosphere [*Fuller-Rowell et al.*, 2010; *Liu et al.*, 2010; *Jin et al.*, 2012] and coupled magnetosphere-ionosphere [*Raeder et al.*, 2001; *W. Wang et al.*, 2004] modeling. In this paper, we treat the thermosphere-ionosphere as one unified geophysical system, and the term "external" refers to anything outside the thermosphere-ionosphere system. Solar and magnetospheric drivers, as well as waves propagating upward from the mesosphere, must then be specified externally to the thermosphere-ionosphere forecasting process.

1.4. Observations

Ground-based dual-frequency Global Positioning System (GPS) receivers currently provide the largest source of ionospheric measurements in the form of integrated electron density along the path from the ground station to the satellite. This is referred to as slant total electron content (TEC). These slant measurements could be directly ingested into the data assimilation scheme used here, but their use would require intensive data preprocessing (bias correction and cycle slip detection) and the development of an experimental three-dimensional covariance localization function that does not currently exist in the Data Assimilation Research Testbed (DART). Such a development would require an understanding of the accuracy of modeled covariances between electron densities at all altitudes and the integrated slant TEC, including the dependence on satellite elevation angle. Therefore, it is more straightforward for us to use vertical TEC values provided by the Massachusetts Institute of Technology (MIT) Haystack observatory. The MIT processing approach, named MAPGPS, was developed by *Coster et al.* [2003] and is explained in detail in *Rideout and*

Coster [2006]. The algorithm detects and corrects cycle slips, applies phase smoothing to the pseudorange observations, and corrects for satellite and receiver biases using a multimethod approach. Slant TEC estimates produced by these steps are converted to vertical TEC values using an adjusted cosine mapping function (adjustment factor = 0.95) and a pierce-point of 450 km. Data are binned into 1° and 5 min averages. In the absence of a published error estimate for this technique, we base our observation error estimate (5 total electron content unit (TECU; 1 TECU = 10^{16} el m^{-2})) on the work of *Hernández-Pajares et al.* [2009], who report standard deviations of 4.42–6.84 TECU for five different vertical GPS TEC algorithms against TOPEX and Jason-1 vertical TEC observations. Those standard deviations include the error due to mapping the TEC reconstruction grid to the locations of TOPEX/Jason-1 data as well as the slant-to-vertical conversion, whereas *Mannucci et al.* [2005] report a slant TEC figure of ~1–3 TECU for data that do not include the mapping and slant-to-vertical errors.

Validation of the assimilation results is performed using two independent data sets—electron density profiles from MIT Haystack and Arecibo Incoherent Scatter Radars (ISRs) and point electron densities from the Langmuir probe on the Challenging Minisatellite Payload (CHAMP) [*Reigber et al.*, 2000]. Millstone Hill is at 42.6°N, 71.5°W, and Arecibo is at 18.4°N, 66.6°W. CHAMP had a polar orbit at approximately 370 km and 360 km altitude in January and September 2005, respectively.

1.5. Data Assimilation

There are a number of approaches to the problem of combining observations with model forecasts (also known as the *background*) to produce *analyses* of the current state of a geophysical system that are referred to as data assimilation techniques. The most common data assimilation techniques are known as 3D-Var, 4D-Var, and ensemble Kalman filters (EnKF) [*Daley*, 1993]. An EnKF is used in this study, and *Evensen* [2003] provides a comprehensive reference for this class of techniques. The EnKF is able to represent temporal variations in the forecast error covariance. The level of confidence in the model forecast is adjusted according to the ensemble spread. Time-dependent spatial and cross-variable correlations of the model forecast errors are also estimated from the model ensemble. For example, if model errors become de-correlated over a given region during a storm then the observations of that region will have less or no impact on the analysis of the surrounding region. EnKFs allow for the incorporation of nonlinear forward operators and inherently produce an ensemble of forecasts that can be used to estimate forecast uncertainty. The primary theoretical limitation of EnKFs, as well as 3D-Var and 4D-Var, is that all errors are assumed to be Gaussian. A number of studies document the relative capabilities of ensemble Kalman filters and variational methodologies [*Lorenc*, 2003; *Kalnay et al.*, 2007; *Buehner et al.*, 2010]. In the EnKF used here, a joint-space localization function is used to reject spurious long-distance covariances, which arise from limited ensemble size and model deficiencies. The covariance is calculated from the difference between each ensemble member and the ensemble mean, then tapered off away from the spatial location of each observation according to the localization function.

Upper atmospheric ensemble data assimilation approaches have been employed by *Codrescu et al.* [2004], *Matsuo and Araujo-Pradere* [2011], *Lee et al.* [2012], *Morozov et al.* [2013], and *Hsu et al.* [2014], while *Scherliess et al.* [2009] have applied the ensemble approach to ionospheric data assimilation. Several existing ionospheric data assimilation efforts estimate neutral parameters (e.g., Global Assimilative Ionospheric Model (GAIM) by *C. Wang et al.* [2004], the Global Assimilation of Ionospheric Measurements (GAIM) by *Schunk et al.* [2004], and the Estimating Model Parameters from Ionospheric Reanalysis approach by *Datta-Barua et al.* [2009]), but these approaches do not treat the thermosphere-ionosphere as a self-consistent, coupled system. It has not been demonstrated that unobserved parameter estimation can improve ionospheric TEC forecasts during storms.

1.6. External Drivers

In order to produce an ensemble of model simulations for a strongly forced and dissipative dynamical system such as the upper atmosphere, it is usually necessary to vary the external driver conditions. *Richmond et al.*'s [1992] Thermosphere Ionosphere Electrodynamics General Circulation Model (TIEGCM), the model used in this study, by default takes in scalar indices (e.g., Kp and $F_{10.7}$) to define drivers such as solar flux, the high-latitude electric field and auroral precipitation. It is possible to produce an ensemble by driving TIEGCM with a range of different values of these indices [e.g., *Lee et al.*, 2012] to produce different model realizations. However, the indices cannot fully characterize disturbed solar and geomagnetic conditions. *Lu et al.* [2008a, 2008b]
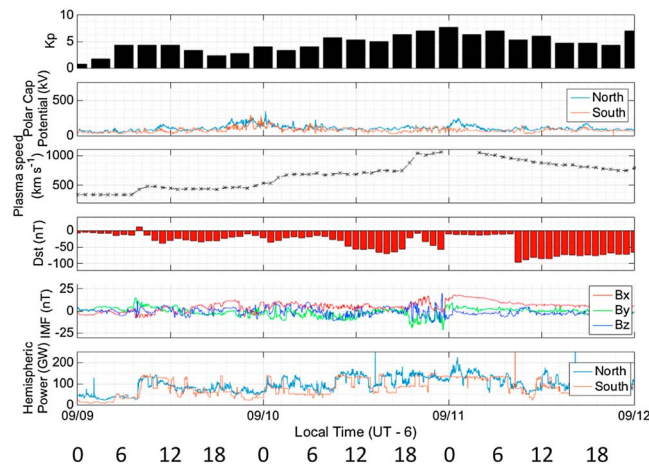
Figure 1. Geomagnetic index (*Kp*), AMIE polar cap potential, disturbance storm time index (*Dst*), Advanced Composition Explorer plasma speed and IMF strength, AMIE hemispheric power from 9 to 12 September 2005.

incorporated far more detailed specifications of these drivers into TIEGCM to simulate the geomagnetic storm that occurred on 10 September 2005. Their model setup, which is used in this study, was in good agreement with measurements of ionospheric electron densities, temperatures, and vertical drifts from Arecibo and Millstone Hill. In their study, the solar flux spectrum observed by the Solar EUV Experiment (SEE) on board the Thermosphere Ionosphere Mesosphere Energetics and Dynamics (TIMED) satellite is used, while high-latitude mean energy, energy flux, cusp latitude, and electric potential are determined by the Assimilative Mapping of Ionospheric

Electrodynamics (AMIE) procedure [*Richmond*, 1992]. The inputs to AMIE include ion drift and particle data from Defense Meteorological Satellite Program F13, 15, and 16; particle data from National Oceanographic and Atmospheric Administration satellites 15, 16, and 17; the Super Dual Auroral Network radar data (ten in the northern hemisphere and two in the southern hemisphere); and from 178 ground magnetometers. The AMIE technique is an assimilative mapping of these observations onto the convection model of *Heelis et al.* [1982] and the conductance model of *Fuller-Rowell and Evans* [1987]. Convection potentials and auroral mean energy and energy flux in both hemispheres from AMIE are saved at 5 min cadence, and then temporally interpolated to drive TIEGCM, which is run at a 2 min time step.

The goal of this study is to determine the effect of TEC assimilation on the accuracy of short-term storm time TEC predictions at midlatitudes. TEC observations are assimilated into a thermosphere-ionosphere model ensemble. One-hour predictions are assessed against observed TEC, electron density profiles from ISRs, and point electron densities from CHAMP. Performance is compared with co-rotated persistence forecasts, and the effects of different assimilation settings are assessed.

1.7. Storm Characteristics

For this investigation, the moderate storm of 10 September 2005 is selected to serve as the primary case study. A second, anomalous storm period (on 22 January 2005) is chosen to test the validity of our conclusions, in which we perform a separate assimilation experiment. We first discuss the context of the September event, followed by the January event. None of the indices shown in Figures 1 and 2 are used in the creation of the ionospheric predictions shown later, although the AMIE values are summaries of the inputs used. Instead, we use multidimensional specifications of solar flux from the Thermosphere Ionosphere Mesosphere Energetics and Dynamics (TIMED) satellite's Solar EUV Experiment (SEE) and two-dimensional high-latitude inputs from AMIE.

The geomagnetic disturbance index, *Kp*, solar wind plasma speed and IMF conditions for the September storm are shown in Figure 1. We define a "local time" (UT—06:00) for the continental USA that is used for consistency with results presented later, and the timing reported by other authors is likewise converted.

Figure 1 shows that solar wind plasma speed increased and the IMF components became more variable in the period after 06:00 LT USA on 9 September. A geomagnetic disturbance of $Kp = 6^-$ occurred in the 06:00–09:00 LT window on 10 September, and the index increased further to 8^- between 21:00–24:00 LT on 10 September. *Goncharenko et al.* [2007] report that an associated ionospheric storm occurred on 10 September 2005, with strong positive phase effects (e.g., enhanced TEC) beginning after 07:00 LT in North America. The authors found that a combination of effects were responsible for the increased ionization. At subauroral and middle latitudes, penetration electric fields acted to increase the plasma density, while a traveling atmospheric/ionospheric disturbance (TAD/TID) and possibly an increased O/N_2 ratio contributed at middle and lower latitudes.
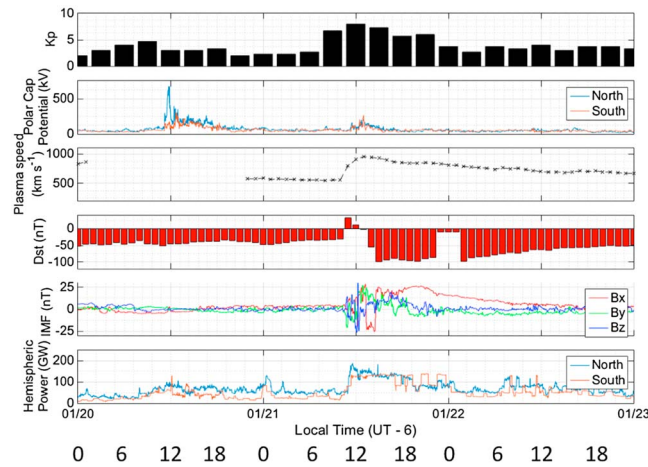
Figure 2. Geomagnetic index (*Kp*), AMIE polar cap potential, disturbance storm time index (*Dst*), Advanced Composition Explorer plasma speed, and IMF strength, AMIE hemispheric power from 20 to 23 January 2005.

Lu et al. [2008a] show that a storm-enhanced density region formed over North America between 12:00–13:00 LT on 10 September. The positive storm phase in North America can be defined to occur between 09:00–18:00 LT. The most disturbed period shown here (19:00 to 23:00 LT on 10 September) coincides with a positive storm phase in the Pacific sector, where there are relatively few ionospheric observations available.

Du et al. [2008] report the occurrence of a major anomalous geomagnetic storm on 21–22 January 2005. The storm is considered highly anomalous because its positive phase coincided with a period of northward IMF conditions. An unusually strong magnetic shock arrived at Earth at about 11:00 LT on 21 January. The same indices shown in Figure 1 are shown for the January event in Figure 2.

Du et al. [2008] define the positive phase of this storm as beginning at 13:46 LT on 21 January, and note that the IMF remains predominantly northward until 19:24 LT. *Sahai et al.* [2011] studied the ionospheric N_mF_2, h_mF_2, and TEC response to the storm in the Latin American sector. The authors noted a strong TEC enhancement near the equator, with relatively weak enhancements at southern midlatitudes. They observed that the main phase ended at about 18:00 LT on 22 January, with N_mF_2 dropping below quiet time levels after that. It is worth noting that their analysis of the storm phases is based in a different geographical region (South and Central America) than our study (continental USA). The anomalous nature of this storm makes it an ideal candidate for testing the robustness of the assimilative predictions presented here.

2. Method

2.1. Driver Perturbations

In order to represent model and external driver uncertainties in the ensemble, we apply random Gaussian perturbations to the SEE and AMIE specifications. These specifications are given in terms of two-dimensional, time-varying fields, so their space-time coherence needs to be taken into account. The variability introduced to the driver specifications is largely heuristic and is described below. Following the approach of *Lee et al.* [2012], 90 randomized versions of the drivers are produced to create the 90 members of the TIEGCM ensemble. Each member is run for 24 h with the randomized drivers to create a set of initial conditions for the assimilation. After that point, observations are assimilated hourly.

Solar flux uncertainties are represented by an ensemble of solar flux time series. Each of these is derived from the SEE observations, which are taken about 15 times daily (once per orbit). Each member is calculated by multiplying the observed time series by a single random number sampled from a zero-mean normal distribution with a standard deviation of 10%. The deviations here are completely correlated across wavelengths and in time. This choice could be seen as representing potential long-term, systematic biases in the instrumentation or in the modeled interpretation of solar flux. One possible alternative would be to introduce time-varying randomizations, but we currently have no reason to believe solar flux-related biases vary temporally.

Four AMIE parameters are required to drive TIEGCM: cusp latitude, mean energy, energy flux, and electric potential. Normal, zero-mean random errors with a standard deviation of 10% are applied to the mean energy and energy flux fields, while random perturbations with a three-degree standard deviation are applied to the cusp latitude parameter. The perturbations applied to these fields and parameters are 100% spatially and temporally correlated, as is the case for the solar flux. The random numbers used are the same for each group of fields, but different across the two hemispheres. The electric potential presents a special set of problems, because the
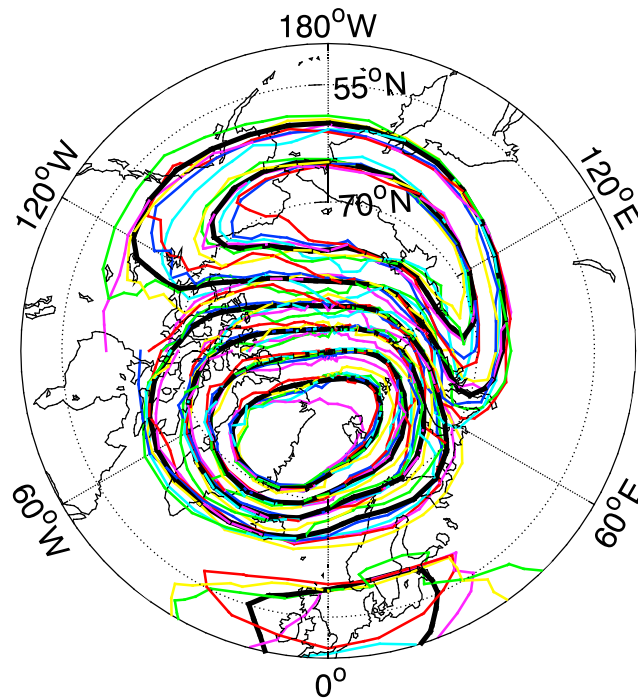
Figure 3. Electric potential at 12:00 LT (18:00 UT) on 10 September 2005 in the Arctic (midday is on the left). Original AMIE map in black and five example perturbations in color.

electric field (the gradient of the potential) is the quantity of importance to the model. If an independent spatiotemporal random noise distribution is applied to the potential, the total electric field strength will be increased. The aim here is to create an ensemble distributed around the AMIE estimate, evolving spatially and temporally to account for uncertainties due to varying coverage. A heuristic choice is made to vary the gradient of the potential at two spatiotemporal scales: one and two thirds degrees and 5 min, and also 10° and 30 min. The AMIE electric field is calculated, randomized at the two spatiotemporal scales, and then translated back to an ensemble of electric potential maps. Each of these variations is sampled from a zero-mean normal distribution with a standard deviation of 30% of the AMIE electric field. Figure 3 shows an example AMIE electric potential perturbation. Drift velocities flow along lines of constant potential, in this case antisunward across the polar cap and returning sunward at lower latitudes.

The solar and geomagnetic drivers are not adjusted by the data assimilation process.

2.2. Specifics of the EnKF Experiments

An ensemble adjustment scheme proposed by *Anderson* [2001] and implemented in the Data Assimilation Research Testbed (DART) [*Anderson et al.*, 2009] is used in this experiment. The configuration used here involves the following steps:

1. An ensemble of TIEGCM initial conditions is produced.
2. Localization of the model error covariance is applied to limit the spatial impact of the observations. A covariance function (a quasi-Gaussian form) proposed by *Gaspari and Cohn* [1999] is used for horizontal localization (on geographic coordinates) around each observation. The localization value is defined as the half-width of that function. No vertical localization is applied.
3. All ensemble forecast members are updated to form an ensemble of analyses according to the ensemble adjustment algorithm [*Anderson*, 2001], and each observation is assimilated sequentially [*Anderson*, 2003]. Note that the forecast (or "background") error covariance is calculated from the differences of the ensemble members to the ensemble mean.
4. Outlier observations are rejected if they fall further than three combined model-observation standard deviations from the prior ensemble mean prediction.
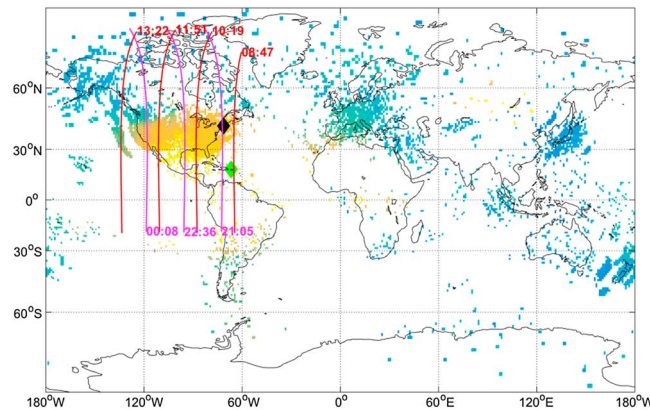
Figure 4. The locations of data used in this study. Five-minute, 1° averages of vertical TEC from ground-based GPS at 13:00 LT (19:00 UT) on 10 September 2005. Relevant segments of CHAMP orbit passes shown in red/pink (northward/southward) with the mean LT of each segment labeled. Millstone Hill and Arecibo observatory are shown as black and green diamonds.

5. The assimilation window is 1 h. Observations within 5 min of each time are assimilated. After the ensemble members are updated, they are run forward for 1 h using the predefined external driver conditions specific to each member.

2.3. The EnKF State Vector

Ideally, all the model state variables (winds, temperatures, composition, etc.) would be included in the EnKF state vector so that they could be modified according to the correlations between the different state variables and each observation. In practice, the modeled covariance exhibits 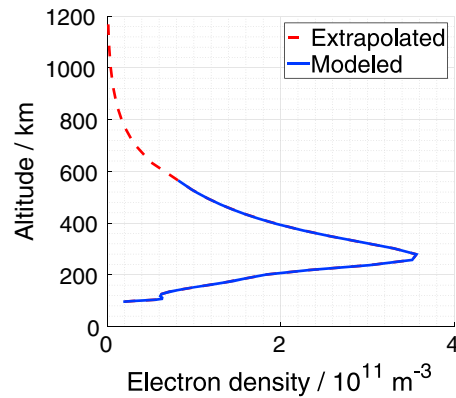spuriously strong correlations between variables and at large distances. The reasons for this are that the model typically produces overly smooth representations of reality, the input driver ensemble is flawed, and there are a limited number of samples in the ensemble. If left unaccounted for, these spurious correlations lead to unjustified modifications of the model state variables. Spatial localization removes spurious long-distance correlations, but does not affect spurious local correlations between different variables. These local correlations are dealt with by including only those variables we believe to be strongly correlated with the observations into the EnKF state vector. Since we are using vertical TEC observations, it is logical to include electron density and O^+ density in the EnKF state vector. As for the thermospheric state variables, the winds and the O/N_2 ratio are included because of their well-known effects on ionospheric density (e.g., *Rishbeth et al.* [2000] for composition effects on F_2-layer density, *Immel et al.* [2001] for O/N_2 enhancements during storms, and *Lu et al.* [2008b] for positive storm driving by neutral winds). Using TIEGCM, the O/N_2 ratio is adjusted by modifying the mixing fraction of O, because the mixing fraction of N_2, referred to here as $[N_2]$, is stored implicitly as follows:

$$[N_2] \,=\, 1 - ([O] + [O_2]) \tag{1}$$

where $[O]$ and $[O_2]$ are the mass mixing fractions of atomic and molecular oxygen. $[O_2]$ is not adjusted in our scheme. It is clearly desirable to specify thermospheric variables as accurately as possible, but it is not obvious that we can infer all of them from TEC observations. Experiments are performed with and without thermospheric variables in the EnKF state vector to elucidate any errors introduced by this process.

2.4. Observations

The observations assimilated here are vertical TEC values preprocessed from ground-based GPS slant TEC by the MIT Haystack Observatory using the method described by *Rideout and Coster* [2006]. Around 4000 globally distributed observations are ingested each hour. ISR and CHAMP electron density observations are also used for model validation. The locations of these observations on 10 September 2005 are shown in Figure 4.

GPS measures TEC from the ground to the altitude of the satellites (around 20,000 km), whereas the top of TIEGCM extends only to about 600 km, depending on solar irradiance. There is a significant contribution to GPS TEC from plasma above 600 km, so a forward operator is used that extrapolates the modeled electron density up five scale heights to around 2500 km, using the assumption of vertical diffusive equilibrium at the top of the model with a constant plasma temperature. There are several problems with this approach. The plasma is not always in diffusive equilibrium, the temperature is not constant, the scale height increases when H^+ becomes the dominant ion, and therefore, there is some plasma above our extrapolation. However, our extrapolation is an improvement over the assumption that there is no plasma above the top of the model. The extrapolation process is shown in Figure 5. In the example shown, the extrapolation accounts for 12% of the total TEC. The extrapolation is moderately sensitive to the plasma temperature at the model top: doubling that temperature adds a further 13% to the total TEC.

Figure 5. Topside extrapolation of electron density 10 levels up from the top of TIEGCM. Extrapolation accounts for plasmaspheric contribution to GPS TEC observations. This profile is from 37.5°N, 100°E, 13:00 LT (19:00 UT) on 10 September 2005.

The standard deviation of the slant-to-vertical GPS TEC observations is set to 5 TECU. This includes errors due to mapping between model and observations. Observations are rejected when the distance between the observation and the model forecast is more than three times the square root of the sum of the observation and model forecast error variances. In practice, around 1.5% of observations are rejected. These "bad" observations are not assimilated but are included in tests of forecast accuracy.

2.5. Experiment Specifics

Assimilative predictions are produced for the January and September storm periods identified in the introduction. The continental USA region (defined as 25°–55°N, 75°–130°W) is chosen for these experiments because it is well covered by observations (see Figure 4) and because *Goncharenko et al.* [2007] identified the importance of plasma density and winds (as TADs/TIDs) and possibly O/N_2 in driving the positive storm phase in this region. These variables are adjusted by the EnKF, whereas the important high-latitude driver (penetration electric fields) is not.

The EnKF allows for unobserved variables to be inferred from observations of other variables, so long as correlations exist between them. *Chartier et al.* [2013] and *Hsu et al.* [2014] showed using simulations that accurate specification of thermospheric composition is particularly important for improving ionospheric forecast accuracy, while the importance of neutral winds during storms is widely acknowledged [e.g., *Buonsanto*, 1999]. *Hsu et al.* [2014] inferred thermospheric parameters from radio occultation observations of electron density in an observing system simulation experiment under geomagnetically quiet conditions. Here assimilation experiments are performed to determine which model state variables can be adjusted to improve ionospheric forecasting, using a real storm case and real observations. The model state variables tested are plasma density, thermospheric composition, and thermospheric winds. The different configurations are as follows:

1. Ionosphere (e^-, O^+)
2. Ionosphere and composition (e^-, O^+, O, N_2)
3. Ionosphere, composition, and winds (e^-, O^+, O, N_2, U, V)
4. Ionosphere and winds (e^-, O^+, U, V)

When observations are assimilated, localization is used to limit the spatial impact of the observations. In our case, joint-space localization is used so as to restrict the covariance to an area defined around each observation as it is assimilated. The localization radius should be set large enough to include realistic correlations, but small enough to reject spurious long-distance correlations. Experiments are performed to determine the optimal localization radius, testing 0.2, 0.5, and 1.0 radians (11.5, 28.6, and 57.3°).

A control run is performed, where no observations are ingested in the model. This run is included to show the effects of the assimilation process. For comparison, 1 h persistence TEC forecasts are produced by rotating the TEC observations on constant geomagnetic latitudes.

3. Results

3.1. Model Bias Against the Observations

Before assimilating observations, it is worth considering the accuracy of the model compared with the observations. The errors of each ensemble member from a dry run (or control run) without assimilation are compared to the TEC observations are shown in Figure 6.

In the lead-up to the storm (up to 07:00 LT), the ensemble has a small positive bias. The positive bias and the ensemble spread grow in the early part of the storm (07:00–12:00 LT) as TEC values increase. The positive bias decreases between 12:00 and 15:00 LT, then recovers until 20:00 LT before subsiding as night falls, indicating
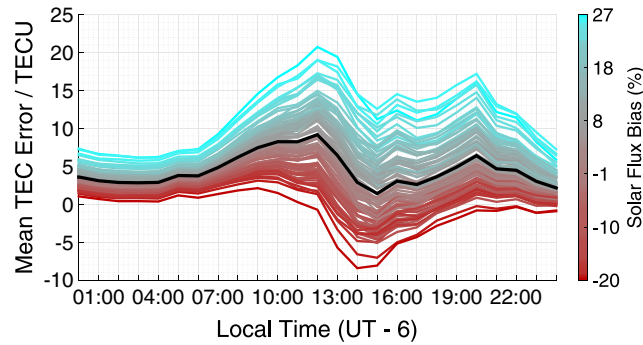
Figure 6. Biases of each dry run ensemble member compared with TEC observations in the continental USA on 10 September 2005. Ensemble mean is shown in black. The color scale shows what bias is applied to the solar flux driving each member.

that the model has an overall positive bias but does not fully represent the positive storm phase. There is a clear correlation between solar flux bias and model TEC in the continental USA, which shows that the solar flux randomization is an important driver of ensemble spread.

3.2. Validation Against TEC

One-hour ensemble mean predictions are compared against TEC observations in Figure 7. The state vector is in configuration (c) (ionosphere, winds, and composition) and a localization radius of 1.0 radians is used.

The prediction reproduces the general trends of the observations, including TEC enhancement of the positive phase of the storm at 13:00 and 15:00 LT. However, the predicted TEC enhancement is less intense and does not extend as far north as what is observed, resulting in an underestimation of up to 12 TECU in the northwestern USA at 13:00 LT. The observed ridge-like enhancement is not represented in the predictions. Given the similarity of this ridge feature to the storm-enhanced density plume observed by *Foster et al.* [2005] using the same GPS technique, the discrepancy may be caused by the lack of a plasmasphere in our model.

3.3. Validation Against Other Observations

So far, we have examined the accuracy of assimilative predictions with respect to verticalized GPS TEC observations. Two other data sets are used here: in situ electron densities from a Langmuir probe on CHAMP, which are available during both periods, and ISR data, which are only available in the September event. The accuracy of the predicted electron density altitude profile is assessed against ISR observations at Millstone Hill and Arecibo in Figure 8. A dry (or control) run with no assimilation is included for comparison.

The results of Figure 8 show that the model reproduces the major features seen at Millstone Hill and at Arecibo. The altitude variations seen at both stations on 10 September are reproduced accurately. The assimilation is effective in reducing the positive bias of the dry run, but the F region electron densities are then underestimated during the positive storm phase on 10 September, while the reverse is true on 9 September. The indication is that the model has most of the physics and accurate initial conditions necessary to reproduce storm time and quiet time behavior at these stations, but it is missing a source of plasma at the peak of the positive phase of the storm. At 16:00 LT at Arecibo the observed N_mF_2 is 2.13×10^{12} e/m^3, which is 49% higher than the predicted value of 1.43×10^{12} e/m^3. The height of the peak density, h_mF_2, is predicted at 297 km versus the observed 330 km, which may indicate that the model is missing some of the plasma-lifting effects of penetration
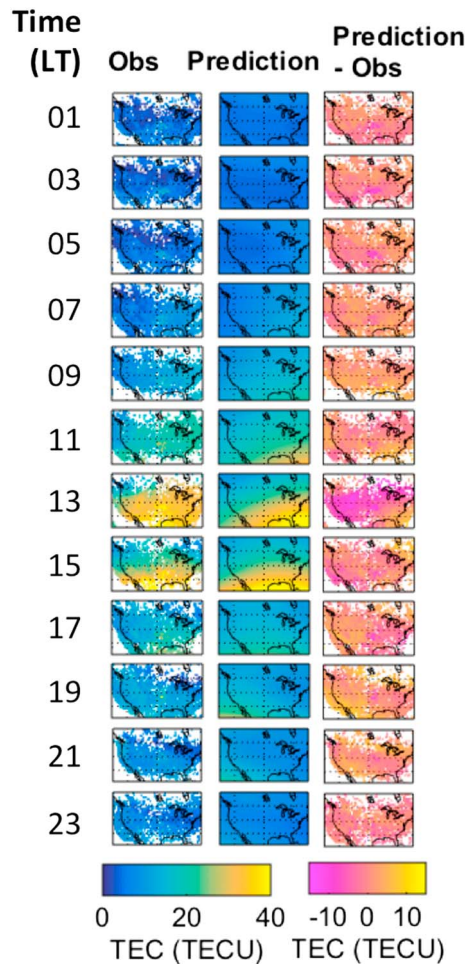

Figure 7. TEC observations, 1 h ensemble mean predictions from run (c) and the differences between the two (prediction-observations) on 10 September 2005.
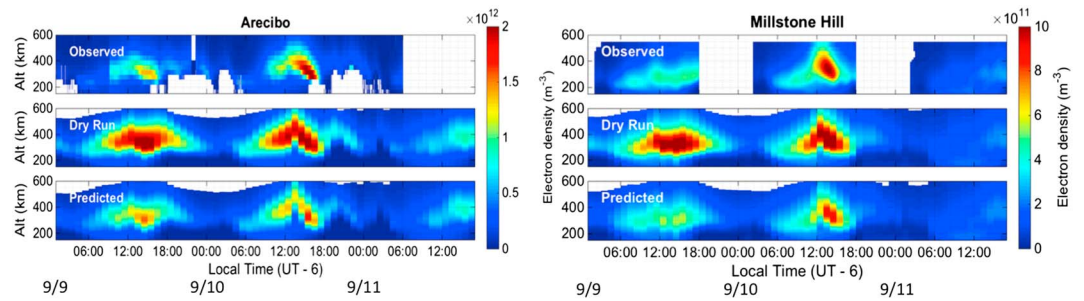
Figure 8. Comparison of ISR observed electron densities from Arecibo and Millstone Hill with the ensemble mean of the dry run and 1 h assimilative prediction (*c*) between 9 and 11 September 2005 (LT).

electric fields and/or equatorward neutral winds, with the result that the plasma recombines too quickly. The overestimated h_mF_2 earlier (13:00 LT: 482 km predicted, 367 km observed) may be an indication that one or both plasma lifting processes acted too early in the model.

CHAMP in situ electron density data are available at 15 s (approximately 120 km) cadence during both periods (21 January and 10 September 2005). These data were provided by the German Research Centre for Geosciences (GFZ Potsdam). The model results are linearly interpolated to the times and locations of the CHAMP observations. Results are shown in Table 1.

The results of the CHAMP comparison show the assimilative prediction corrects most of the electron density bias of the dry run (18.7% down from 55.4% on 22 January, 6.7% down from 26.7% on 10 September). However, the assimilation does not correct the RMS error, indicating that the model is still unable to reproduce the observed variability accurately.

3.4. Comparison With Corotated Predictions

The accuracy of 1 h ensemble mean TEC predictions and persistence forecasts is shown in Figure 9. The anomalous storm of January 2005 is included in this comparison. Persistence forecasts are made by corotating observations on constant geomagnetic latitudes an hour forward in time. The persistence forecasts are compared against observations within 1° of their new locations. Configuration (c) is again used for the assimilation.

The January storm is more intense than the one in September, so it is logical that prediction errors are much larger. The dry run is the least accurate in both cases and has large positive biases during the day. The analysis is most accurate in both cases because it has access to the observations being compared against here. Analysis RMS error growth in the main phases indicates the inherent weakness of a 5° resolution model in matching 1° binned observations during disturbed times. The 1 h prediction is far more accurate than the dry run, indicating that TEC assimilation is effective in reducing model errors over short prediction periods, even during storms. However, the prediction error is still much larger than the analysis, which indicates the need for improved specification of the model's magnetospheric and solar drivers.

The persistence forecast is useful as a performance benchmark, although it is possible that it shares a common bias with the observations. Before the storms, the persistence matches the observations better than the assimilative prediction. The persistence errors increase in the later part of the main phase and the recovery phase, whereas the assimilative prediction has larger errors in the early part of the main phase and the buildup to the January storm. In the 10 September recovery phase, the assimilative prediction bias remains above the baseline, which is not the case in January. The 10 September recovery effect may be caused by the buildup to the 11 September storm that occurs at about midnight LT.

Table 1. Comparison of Model Runs Against CHAMP In Situ Electron Densities in Continental USA

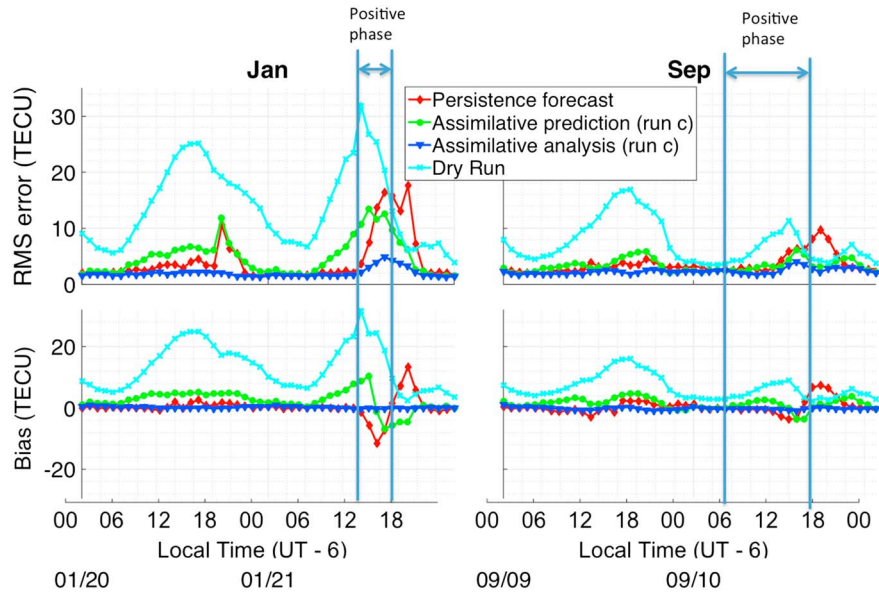|	21 January (Local Time)		10 September (Local Time)	
	Dry Run	1 h prediction	Dry Run	1 h prediction
Bias (%)	55.4	18.7	26.7	6.7
RMS (%)	73.7	71.9	64.3	64.4

Figure 9. RMS TEC errors and biases of a 1 h persistence forecast (red), 1 h ensemble mean assimilative prediction (green) and analysis (dark blue) from configuration (*c*), and a dry run with no assimilation (light blue). The positive storm phases shown are defined according to *Sahai et al.* [2011] for January, and *Goncharenko et al.* [2007] for September.

3.5. Effect of State Variables

A state vector including multiple unobserved variables and a large localization radius was used in the previous experiments. The effects of these choices are analyzed in this and the next section. Experiments are performed with four combinations of state vector variables (*a*, *b*, *c*, and *d* as described above). The localization radius is set to 0.5 radians (28.6°) for these experiments. Figure 10 shows the RMS errors of 1 h predictions from the four runs against vertical TEC observations.

All state vector configurations have similar performance. The bias seen in the control run (in Figure 6) is seen again here, indicating the important influence of external (solar and geomagnetic) drivers on the ionosphere during storms. The ionospheric assimilation (*a*) is less effective in reducing the positive bias between 06:00 and 12:00 LT. However, the stronger bias corrections introduced by modifying the composition in runs (*b*) and (*c*) have the effect of causing a larger negative bias between 13:00 and 15:00 LT. Run (*b*) is more similar to run (*c*) than runs (*a*) and (*d*), indicating that including O/N2 in the state has a stronger effect on model evolution than including the winds, as was reported by *Chartier et al.* [2013] and *Hsu et al.* [2014].
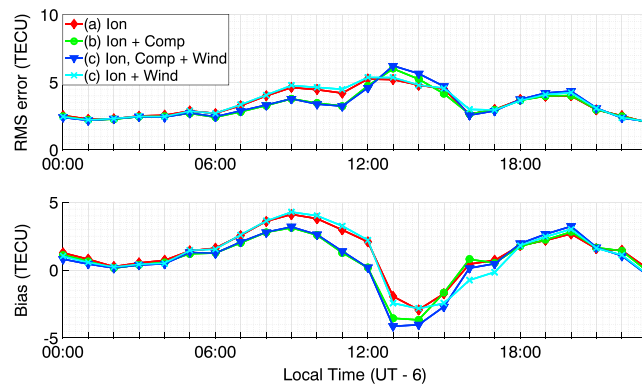

Figure 10. RMS TEC errors and biases of four 1 hour predictive assimilation runs in the continental USA are shown for 10 September 2005. The effect of including different variables in the state vectors is addressed here.

3.6. Localization

The localization radius should be set to the distance within which the ensemble can produce reliable estimates of the error covariances between state variables. A perfect ensemble would function best with an infinite localization radius because it would specify covariances accurately at all distances, but in practice the ensemble can produce spurious covariances at long distances from the observations. Figure 11 shows the effects of different localization radii on our results.

Before 12:00 LT, there is no appreciable difference between the three runs,
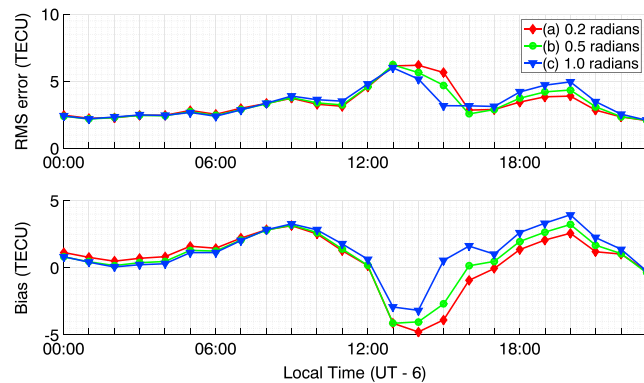
Figure 11. RMS TEC errors and biases of three 1 h predictive assimilation runs in the continental USA are shown for 10 September 2005. The effect of different localization radii is addressed here.

perhaps indicating that long-distance correlations are unimportant or unnecessary in this period. Between 12:00–15:00 LT the largest localization radius run (*c*) performs best, but the situation is reversed after that. This could be an indication that the ensemble does not properly represent the variability in the later stages of the storm.

4. Discussion

Assimilation of TEC observations is effective in reducing the RMS error and bias of 1 hour TEC predictions in the Continental USA during two storm periods. The related electron density bias is also reduced against CHAMP and ISR data, although the CHAMP analysis does not show an improvement in RMS error (perhaps due to the limited model resolution). Before the storms, and during part of the main phase, a persistence forecast is more accurate than the assimilative prediction, whereas the assimilation is more accurate in the later part of the main phases and the recovery phase. The improvement against the background shows that TEC assimilation can play an important role in correcting biases in short-term predictions, but accurate initial conditions alone are not sufficient to produce accurate predictions. The magnetospheric and solar drivers are important even on short time scales, so a successful physics-based prediction approach must include either some capacity for predictive estimation of forcing parameters, or use an integrated magnetosphere-ionosphere approach where the full system can be specified accurately. The thermosphere-ionosphere system exhibits rapid variability during storms, so it is possible that an assimilation cadence faster than 1 h will also provide some improvement. Such an approach has to take into account the risk of destabilizing the model through rapid updates.

The results show the effects of including different variables in the state vector. As was shown theoretically by *Chartier et al.* [2013] and in an observation system simulation experiment by *Hsu et al.* [2014], changes to the thermospheric composition (O/N$_2$ in this case) have more impact on the model prediction than changes to the winds. This is not to say that neutral composition is more important than winds in driving positive storm effects. Instead, the result indicates that the composition responds more slowly than the winds to forcing from other parameters, so its effects are seen to last longer. Since both parameters are known to be important components of storm time ionospheric behavior, it is clearly desirable to specify them accurately. For composition, this should be achievable through direct assimilation of observations. The situation is more complex for winds, because they respond more quickly to external forcings such as high-latitude heating from precipitation and convection. *Morozov et al.* [2013] and *Matsuo et al.* [2013] demonstrated that it is possible to infer solar and geomagnetic drivers from thermospheric observations using an EnKF. Estimation of solar and geomagnetic drivers using TEC observations will be addressed in future work.

The analysis RMS error growth seen during the positive phase of the storms indicates that the 5° model resolution cannot fit the variability seen in 1°-binned observations at these times. The indication is that a higher-resolution model is required in these periods. This may have serious consequences for ensemble approaches, where the computing power required by large models can limit the number of ensemble members used. Currently, the single-threaded TIEGCM configuration runs fast enough that the ensemble size can be set as large as is deemed useful, given the state-of-the-art high-performance computing facilities available. Of course, it is desirable to use more complex models that represent all the important regions at high resolution, such as the magnetosphere and the lower atmosphere, but those models require far more computing resources with the consequence that smaller ensembles must typically be used. One alternative is to use single-threaded approaches such as 4D-Var, while another possibility is to pursue nested-grid approaches in cases where only a regional analysis is required.

In order to generate ensemble predictions of an ionospheric storm, it is necessary to create an ensemble of external drivers that reflects the real uncertainty in the driver specifications. We did not have access to forecasts

of the drivers used in this study so we added uncertainties to the observed/assimilated values of multidimensional fields such as high-latitude electric potential, particle precipitation and the solar flux spectrum. This approach allows for small-scale variability to be introduced to otherwise overly smooth external driver specifications. An alternative would be to use forecasts of simple, one-dimensional indices such as Kp [e.g., *Wing et al.*, 2005] and $F_{10.7}$ [e.g., *Henney et al.*, 2012]. That approach was not chosen for this study because models are unable to reproduce storms accurately even with measured values of those indices, as was shown by the Community Coordinated Modeling Center challenge studies [*Shim et al.*, 2011; *Emery et al.*, 2012].

Pre-processed, verticalized TEC observations are used in this experiment. This approach is suboptimal because the slant-to-vertical translation introduces errors. A more rigorous approach would be to calculate the modeled values of slant TEC by integrating through the modeled electron density field along a straight path between satellite and receiver and to assimilate the slant TEC data directly. This approach will remove much of the observational error, but instrumental biases are still present in GNSS slant TEC observations. To remove these biases, it would be advantageous to use an algorithm that accommodates time-differenced phase observations, as has been done by *Mitchell and Spencer* [2003].

5. Conclusions

Verticalized GPS TEC observations have been assimilated into a coupled thermosphere-ionosphere model. Model accuracy is improved so that 1 h predictions are more accurate than a 1 h persistence forecast between 11:00 and 18:00 LT on 10 September 2005 in the continental USA. However the persistence forecast is more accurate outside the storm period. The results show the potential for ionosphere-thermosphere assimilation to improve midlatitude storm time TEC forecasting efforts, but also highlight the need for better models and more accurate forecasts of the external drivers.

This study shows that assimilation of TEC observations can be used to improve storm time predictions of ionospheric TEC. The ensemble approach provides both a forecast of the ionosphere and an estimate of forecast uncertainty. Following the approach of *Wang et al.* [1999], mesoscale models could be embedded in an ensemble of large-scale forecasts to provide probabilistic predictions of small-scale effects such as scintillation. The system demonstrated here includes a coupled thermosphere, so it could also form the basis of a satellite drag forecast system [e.g., *Matsuo et al.*, 2013].

References

Anderson, J., T. Hoar, K. Raeder, H. Liu, N. Collins, R. Torn, and A. Avellano (2009), The data assimilation research testbed: A community facility, *Bull. Am. Meteorol. Soc.*, *90*(9), 1283–1296.

Anderson, J. L. (2001), An ensemble adjustment Kalman filter for data assimilation, *Mon. Weather Rev.*, *129*(12), 2884–2903.

Anderson, J. L. (2003), A local least squares framework for ensemble filtering, *Mon. Weather Rev.*, *131*(4), 634–642.

Borries, C., J. Berdermann, N. Jakowski, and V. Wilken (2015), Ionospheric storms—A challenge for empirical forecast of the total electron content, *J. Geophys. Res. Space Physics*, *120*, 3175–3186, doi:10.1002/2015JA020988.

Buehner, M., P. L. Houtekamer, C. Charette, H. L. Mitchell, and B. He (2010), Intercomparison of Variational Data Assimilation and the Ensemble Kalman Filter for Global Deterministic NWP. Part I: Description and Single-Observation Experiments, *Mon. Weather Rev.*, *138*, 1550–1566, doi:10.1175/2009MWR3157.1.

Buonsanto, M. J. (1999), Ionospheric storms—A review, *Space Sci. Rev.*, *88*(3–4), 563–601.

Cander, L. R. (2015), Forecasting foF2 and MUF (3000) F2 ionospheric characteristics–A challenging space weather frontier, *Adv. Space Res.*, *56*(9), 1973–1981.

Chartier, A. T., D. R. Jackson, and C. N. Mitchell (2013), A comparison of the effects of initializing different thermosphere-ionosphere model fields on storm time plasma density forecasts, *J. Geophys. Res. Space Physics*, *118*, 7329–7337, doi:10.1002/2013JA019034.

Codrescu, M. V., T. J. Fuller-Rowell, and C. F. Minter (2004), An ensemble-type Kalman filter for neutral thermospheric composition during geomagnetic storms, *Space Weather*, *2*, S11003, doi:10.1029/2004SW000088.

Coster, A. J., J. C. Foster, and P. J. Erickson (2003), Space weather: Monitoring the ionosphere with GPS, *GPS World*, *14*(5), 42–49.

Daley, R. (1993), *Atmospheric Data Analysis*, Cambridge Univ. Press, Cambridge, U. K.

Datta-Barua, S., G. S. Bust, G. Crowley, and N. Curtis (2009), Neutral wind estimation from 4-D ionospheric electron density images, *J. Geophys. Res.*, *114*, A06317, doi:10.1029/2008JA014004.

Du, A. M., B. T. Tsurutani, and W. Sun (2008), Anomalous geomagnetic storm of 21–22 January 2005: A storm main phase during northward IMFs, *J. Geophys. Res.*, *113*, A10214, doi:10.1029/2008JA013284.

Emery, B. A., et al. (2012), Climatology Assessment of ionosphere/thermosphere models in low solar flux conditions for the CCMC CEDAR challenge, Abstract SA23A-2152 presented at 2012 Fall Meeting, AGU.

Evensen, G. (2003), The ensemble Kalman filter: Theoretical formulation and practical implementation, *Ocean Dyn.*, *53*(4), 343–367.

Foster, J. C., et al. (2005), Multiradar observations of the polar tongue of ionization, *J. Geophys. Res.*, *110*, A09S31, doi:10.1029/2004JA010928.

Fuller-Rowell, T., F. Wu, R. Akmaev, T. W. Fang, and E. Araujo-Pradere (2010), A whole atmosphere model simulation of the impact of a sudden stratospheric warming on thermosphere dynamics and electrodynamics, *J. Geophys. Res.*, *115*, A00G08, doi:10.1029/2010JA015524.

Fuller-Rowell, T. J., and D. S. Evans (1987), Height-integrated Pedersen and Hall conductivity patterns inferred from the TIROS-NOAA satellite data, *J. Geophys. Res.*, *92*(A7), 7606–7618.

Fuller-Rowell, T. J., D. Rees, S. Quegan, R. J. Moffett, M. V. Codrescu, and G. H. Millward (1996), A coupled thermosphere-ionosphere model (CTIM), *STEP Report*, *239*.

Gaspari, G., and S. E. Cohn (1999), Construction of correlation functions in two and three dimensions, *Q. J. R. Meteorol. Soc.*, *125*(554), 723–757.

Goncharenko, L. P., J. C. Foster, A. J. Coster, C. Huang, N. Aponte, and L. J. Paxton (2007), Observations of a positive storm phase on September 10, 2005, *J. Atmos. Sol. Terr. Phys.*, *69*(10), 1253–1272.

Habarulema, J. B., L.-A. McKinnell, and B. D. L. Opperman (2011), Regional GPS TEC modeling: Attempted spatial and temporal extrapolation of TEC using neural networks, *J. Geophys. Res.*, *116*, A04314, doi:10.1029/2010JA016269.

Heelis, R. A., J. K. Lowell, and R. W. Spiro (1982), A model of the high-latitude ionospheric convection pattern, *J. Geophys. Res.*, *87*(A8), 6339–6345.

Henney, C. J., W. A. Toussaint, S. M. White, and C. N. Arge (2012), Forecasting $F_{10.7}$ with solar magnetic flux transport modeling, *Space Weather*, *10*, S02011, doi:10.1029/2011SW000748.

Hernández-Pajares, M., et al. (2009), The IGS VTEC maps: A reliable source of ionospheric information since 1998, *J. Geod.*, *83*(3–4), 263–275.

Hsu, C. T., T. Matsuo, W. Wang, and J. Y. Liu (2014), Effects of inferring unobserved thermospheric and ionospheric state variables by using an Ensemble Kalman Filter on global ionospheric specification and forecasting, *J. Geophys. Res. Space Physics*, *119*, 9256–9267, doi:10.1002/2014JA020390.

Immel, T. J., G. Crowley, J. D. Craven, and R. G. Roble (2001), Dayside enhancements of thermospheric O/N2 following magnetic storm onset, *J. Geophys. Res.*, *106*(A8), 15,471–15,488.

Jakowski, N., C. Mayer, M. M. Hoque, and V. Wilken (2011), Total electron content models and their use in ionosphere monitoring, *Radio Sci.*, *46*, RS0D18, doi:10.1029/2010RS004620.

Jin, H., Y. Miyoshi, D. Pancheva, P. Mukhtarov, H. Fujiwara, and H. Shinagawa (2012), Response of migrating tides to the stratospheric sudden warming in 2009 and their effects on the ionosphere studied by a whole atmosphere-ionosphere model GAIA with COSMIC and TIMED/SABER observations, *J. Geophys. Res.*, *117*, A10323, doi:10.1029/2012JA017650.

Kalnay, E. (2003), *Atmospheric Modeling, Data Assimilation, and Predictability*, Cambridge Univ. Press, Cambridge, U. K.

Kalnay, E., H. Li, T. Miyoshi, S.-C. Yang, and J. Ballabrea-Poy (2007), 4-D-Var or ensemble Kalman filter?, *Tellus A*, *59*, 758–773, doi:10.1111/j.1600-0870.2007.00261.x.

Lee, I. T., et al. (2012), Assimilation of FORMOSAT-3/COSMIC electron density profiles into a coupled thermosphere/ionosphere model using ensemble Kalman filtering, *J. Geophys. Res.*, *117*, A10318, doi:10.1029/2012JA017700.

Liu, H. L., et al. (2010), Thermosphere extension of the whole atmosphere community climate model, *J. Geophys. Res.*, *115*, A12302, doi:10.1029/2010JA015586.

Lorenc, A. C. (2003), The potential of the ensemble Kalman fi filter for NWP—A comparison with 4D-Var, *Q. J. R. Meteorol. Soc.*, *129*, 3183–3203.

Lu, G., L. P. Goncharenko, A. J. Coster, A. D. Richmond, R. G. Roble, N. Aponte, and L. J. Paxton (2008a), A data-model comparative study of ionospheric positive storm phase in the midlatitude F region, in *Midlatitude Ionospheric Dynamics and Disturbances*, edited by P. M. Kintner et al., AGU, Washington, D. C., doi:10.1029/181GM07.

Lu, G., L. P. Goncharenko, A. D. Richmond, R. G. Roble, and N. Aponte (2008b), A dayside ionospheric positive storm phase driven by neutral winds, *J. Geophys. Res.*, *113*, A08304, doi:10.1029/2007JA012895.

Mannucci, A. J., B. T. Tsurutani, B. A. Iijima, A. Komjathy, A. Saito, W. D. Gonzalez, F. L. Guarnieri, J. U. Kozyra, and R. Skoug (2005), Dayside global ionospheric response to the major interplanetary events of October 29–30, 2003 "Halloween Storms", *Geophys. Res. Lett.*, *32*, L12S02, doi:10.1029/2004GL021467.

Matsuo, T., and E. A. Araujo-Pradere (2011), Role of thermosphere-ionosphere coupling in a global ionospheric specification, *Radio Sci.*, *46*, RS0D23, doi:10.1029/2010RS004576.

Matsuo, T., I.-T. Lee, and J. L. Anderson (2013), Thermospheric mass density specification using an ensemble Kalman filter, *J. Geophys. Res. Space Physics*, *118*, 1339–1350, doi:10.1002/jgra.50162.

McNamara, L. F., D. T. Decker, J. A. Welsh, and D. G. Cole (2007), Validation of the Utah State University Global Assimilation of Ionospheric Measurements (GAIM) model predictions of the maximum usable frequency for a 3000 km circuit, *Radio Sci.*, *42*, RS3015, doi:10.1029/2006RS003589.

Mitchell, C. N., and P. S. J. Spencer (2003), A three-dimensional time-dependent algorithm for ionospheric imaging using GPS, *Ann. Geophys.*, *46*(4), 687–696.

Morozov, A. V., A. J. Ridley, D. S. Bernstein, N. Collins, T. J. Hoar, and J. L. Anderson (2013), Data assimilation and driver estimation for the Global Ionosphere–Thermosphere Model using the Ensemble Adjustment Kalman Filter, *J. Atmos. Sol. Terr. Phys.*, *104*, 126–136.

Pi, X., C. Wang, G. A. Hajj, G. Rosen, B. D. Wilson, and G. J. Bailey (2003), Estimation of **E** × **B** drift using a global assimilative ionospheric model: An observation system simulation experiment, *J. Geophys. Res.*, *108*(A2), 1075, doi:10.1029/2001JA009235.

Raeder, J., Y. L. Wang, T. J. Fuller-Rowell, and H. J. Singer (2001), Global simulation of magnetospheric space weather effects of the Bastille Day storm, *Sol. Phys.*, *204*(1–2), 323–337.

Reigber, C., H. Lühr, and P. Schwintzer (2000), Status of the CHAMP mission, in *Towards an Integrated Global Geodetic Observing System (IGGOS)*, pp. 63–65, Springer, Berlin.

Richmond, A. D. (1992), Assimilative mapping of ionospheric electrodynamics, *Adv. Space Res.*, *12*(6), 59–68.

Richmond, A. D., E. C. Ridley, and R. G. Roble (1992), A thermosphere/ionosphere general circulation model with coupled electrodynamics, *Geophys. Res. Lett.*, *19*, 601–604.

Rideout, W., and A. Coster (2006), Automated GPS processing for global total electron content data, *GPS Solut.*, doi:10.1007/s10291-006-0029-5.

Ridley, A. J., Y. Deng, and G. Toth (2006), The global ionosphere–thermosphere model, *J. Atmos. Sol. Terr. Phys.*, *68*(8), 839–864.

Rishbeth, H., I. C. F. Müller-Wodarg, L. Zou, T. J. Fuller-Rowell, G. H. Millward, R. J. Moffett, D. W. Idenden, and A. D. Aylward (2000), Annual and semiannual variations in the ionospheric F2-layer: II. Physical discussion, *Ann. Geophys.*, *18*(8), 945–956.

Roble, R. G., E. C. Ridley, A. D. Richmond, and R. E. Dickinson (1988), A coupled thermosphere/ionosphere general circulation model, *Geophys. Res. Lett.*, *15*(12), 1325–1328.

Sahai, Y., et al. (2011), Studies of ionospheric F-region response in the Latin American sector during the geomagnetic storm of 21–22 January 2005, *Ann. Geophys.*, *29*(5), 919–929.

Scherliess, L., D. C. Thompson, and R. W. Schunk (2009), Ionospheric dynamics and drivers obtained from a physics-based data assimilation model, *Radio Sci.*, *44*, RS0A32, doi:10.1029/2008RS004068.

Schunk, R. W., et al. (2004), Global Assimilation of Ionospheric Measurements (GAIM), *Radio Sci.*, *39*, RS1S02, doi:10.1029/2002RS002794.

Shim, J. S., et al. (2011), CEDAR Electrodynamics Thermosphere Ionosphere (ETI) challenge for systematic assessment of ionosphere/thermosphere models: NmF2, hmF2, and vertical drift using ground-based observations, *Space Weather*, *9*, S12003, doi:10.1029/2011SW000727.

Tulunay, E., E. T. Senalp, S. M. Radicella, and Y. Tulunay (2006), Forecasting total electron content maps by neural network technique, *Radio Sci.*, *41*, RS4016, doi:10.1029/2005RS003285.

Wang, C., G. Hajj, X. Pi, I. G. Rosen, and B. Wilson (2004), Development of the global assimilative ionospheric model, *Radio Sci.*, *39*, RS1S06, doi:10.1029/2002RS002854.

Wang, W., T. L. Killeen, A. G. Burns, and R. G. Roble (1999), A high-resolution, three-dimensional, time dependent, nested grid model of the coupled thermosphere–ionosphere, *J. Atmos. Sol. Terr. Phys.*, *61*(5), 385–397.

Wang, W., M. Wiltberger, A. G. Burns, S. Solomon, T. L. Killeen, N. Maruyama, and J. Lyon (2004), Initial results from the CISM coupled magnetosphere-ionosphere-thermosphere (CMIT) model: Thermosphere ionosphere responses, *J. Atmos. Sol. Terr. Phys.*, *66*, 1425–1442, doi:10.1016/j.jastp.2004.04.008.

Wing, S., J. R. Johnson, J. Jen, C.-I. Meng, D. G. Sibeck, K. Bechtold, J. Freeman, K. Costello, M. Balikhin, and K. Takahashi (2005), Kp forecast models, *J. Geophys. Res.*, *110*, A04203, doi:10.1029/2004JA010500.

Erratum